Out-of-plane spin-orientation dependent magnetotransport properties in the anisotropic helimagnet Cr_{1/3}NbS_{2}

Alexander C. Bornstein, Benjamin J. Chapman, Nirmal J. Ghimire, David G. Mandrus, David S. Parker, and Minhyea Lee

Out-of-Plane Spin-Orientation Dependent Magnetotransport Properties in the Anisotropic Helimagnet Cr$_{1/3}$NbS$_2$

Alexander C. Bornstein,[1] Benjamin J. Chapman,[1] Nirmal J. Ghimire[†],[2,3]
David G. Mandrus,[2,3,4] David S. Parker,[3] and Minhyea Lee[1,*]

[1]*Department of Physics, University of Colorado, Boulder, CO 80309, USA*
[2]*Department of Physics and Astronomy, The University of Tennessee, Knoxville, Tennessee 37996, USA*
[3]*Materials Science and Technology Division, Oak Ridge National Laboratory, Oak Ridge, Tennessee 37831, USA*
[4]*Department of Materials Science and Engineering,*
The University of Tennessee, Knoxville, TN 37996, USA
(Dated: April 13, 2015)

Understanding the role of spin-orbit coupling (SOC) has been crucial to controlling magnetic anisotropy in magnetic multilayer films. It has been shown that electronic structure can be altered via interface SOC by varying the superlattice structure, resulting in spontaneous magnetization perpendicular or parallel to the plane. In lieu of magnetic thin films, we study the similarly anisotropic helimagnet Cr$_{1/3}$NbS$_2$, where the spin polarization direction, controlled by the applied magnetic field, can modify the electronic structure. As a result, the direction of spin polarization can modulate the density of states, and in turn affect the in-plane electrical conductivity. In Cr$_{1/3}$NbS$_2$, we found an enhancement of in-plane conductivity when the spin polarization is out-of-plane, as compared to in-plane spin polarization. This is consistent with the increase of density of states near the Fermi energy at the same spin configuration, found from first principles calculations. We also observe unusual field dependence of the Hall signal in the same temperature range. This is unlikely to originate from the non-collinear spin texture, but rather further indicates strong dependence of electronic structure on spin orientation relative to the plane.

PACS numbers:

Despite the fact that its typical energy scale in $3d$ ferromagnetic metals is small compared to other relevant scales such as band widths, SOC mixes the nature of the spin and orbital components of the Bloch state in a nontrivial way and leads to a variety of electrical transport phenomena e.g. the anomalous Hall effect (AHE), anisotropic magnetoresistance (AMR), and the planar Hall effect. In addition, the recent work in non-collinear magnetically ordered states and the related topological Hall effect [1–3] not only has renewed the pivotal role of SOC through the Dzyaloshinskii-Moriya (DM) interaction [4–6], but also has presented a possibility to employ these findings for functional components in magnetic devices [7, 8]. Non-collinear magnetic ordering is also suggested to possibly manifest spin-orbit coupling in a complex manner, through the DM interaction[6, 9, 10]. Consequently, the modification of electronic structure by spin-orbit coupling is expected to make in-plane electrical transport sensitive to the magnetization orientation relative to the plane.

Cr$_{1/3}$NbS$_2$ has a layered crystalline structure, in which $3d$ transition metal Cr atoms are intercalated in the hexagonal $2H$-type NbS$_2$ matrix as trivalent ions and magnetically order at $T_C = 133$ K. The ferromagnetic layers of Cr^{3+} lie coplanar with the crystallographic ab-planes and the magnetic helix propagates along the c-axis with a long pitch of 48 nm, corresponding to 40 unit cells [11]. Its helimagnetic ordering is attributed to the DM interaction, which originates from a broken inversion symmetry shared by all members of space group $P6_322$

[11–13]. With application of a magnetic field (H) along the ab-plane, *i.e.* perpendicular to the helical axis, ferromagnetic domains are created between the winds of the helix, increasing the length of the magnetic unit cell and forming the chiral soliton lattice phase [14]. As field is increased, all spins become polarized at $H_p^{ab} = 0.18$ T. Alternatively, when H is applied along the c-axis, *i.e.* along the direction of the helical wave vector, the helices smoothly evolve through a conical state. The conical angle decreases with increasing H until polarization at $H_p^c = 2.5$ T [11, 13]. Its electrical conduction is quasi two-dimensional: the electrical resistivity measured with current flowing along the c-axis is in the order of $10^1 - 10^2$ times larger than with current in the ab-plane [11, 15]. In these regards, Cr$_{1/3}$NbS$_2$ displays similar magnetic and structural anisotropies as fabricated planar devices.

So far, SOC in magnetic multilayers or superlattice has been studied intensively in terms of engineering the electronic structure in order to control the spontaneous magnetic anisotropy [16–18, 18–21]. Here, we demonstrate the reverse process in a similarly anisotropic layered system Cr$_{1/3}$NbS$_2$, such that the spin polarization direction controlled by applied magnetic field alters the electronic structure via SOC. For spin polarization along the c-axis, this results in enhanced electrical conductivity, by increasing the DOS near the Fermi surface, as supported by our first principles calculations. This observation is the most prominent for temperatures $T < T_A$; T_A is the temperature scale below which spin-disorder scattering contributes negligibly to the resistance, and

is empirically determined from the temperature dependence of the magnetoresistance. Surprisingly, roughly the same temperature scale of T_A was found in the transverse Hall resistivity, and is also consistent with the onset of deviation from Bloch's $T^{3/2}$ law for the magnetization [13]. While T_A is a crossover temperature and is not sharply defined, it corresponds to the energy scale associated with modifications of the electronic structure, and is thus a useful quantity to estimate.

Single crystals of $Cr_{1/3}NbS_2$ were grown by vapor-transport (see Ref. [11] for details on growth and sample characterization). Crystals from two different batches were used in this study, and show slightly different T_Cs of 120 K and 133 K, but otherwise exhibit very little qualitative difference in the T and H dependences of both electrical and magnetic measurements. All the data presented in this letter are from the sample with $T_C = 133$ K. Samples from both batches were characterized with x-ray diffraction for the crystalline structure and small angle neutron scattering to verify the helimagnetic ground state [22]. Magnetization was measured in a superconducting quantum interference device magnetometer. Electrical transport properties were studied using standard four-probe measurements on samples with typical area $\approx 2 \times 0.3$ mm^2 and thickness $\approx 20 - 70$ μm. Electrical contacts, made by silver paint, had typical contact resistance less than 1 Ω. Rotation of the sample in a field was performed by a home-built rotation probe, which was inserted in a superconducting split coil magnet. For transport measurements, currents of $2 - 4$ mA were applied in the ab plane. The magnetization measurements were performed using SQUID. We used small wedges made of stycast epoxy with various angles to mount the samples under angled magnetic field in magnetization measurements. For the Hall measurement, we checked the uniformity of the current flow by using multiple sets of electric contacts within a sample. The Hall data is antisymmetrized in order to remove magnetoresistance component caused by a slight misalignment of the contacts.

The measurement is configured such that the flow of current lies within the crystallographic ab-plane, while the saturated magnetization sweeps the out-of-plane polar angle from $\theta_H = 0$ to 90° (see the inset of Fig.2 (a)). This corresponds to the out-of-plane anisotropic magnetoresistance configuration as shown in [23, 24]. It is distinct from the typical AMR configuration where both current and the magnetization lie within the film plane [25]. Note that the direction of current *always* remains within the ab-plane and therefore, when $\theta_H = 90°$ the current is parallel to H.

First, we plot the in-plane resistivities (ρ) as a function of H for $\theta_H = 0$ (thick lines) and $\theta_H = 90°$ (thin lines) at different fixed temperatures (T) in Fig. 1(a) and (b). Fig.1(c) summarizes the T dependence of the in-plane magnetoresistance (MR), defined as $\Delta\rho/\rho_0 =$
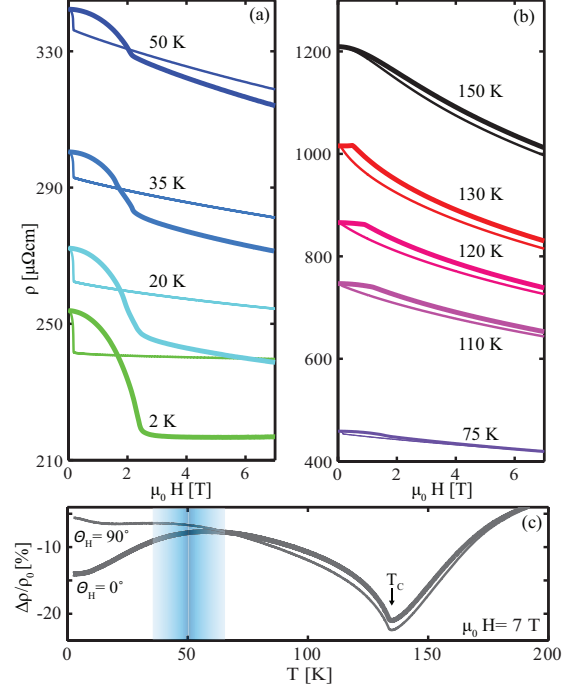

FIG. 1: (a,b) In-plane resistivity ρ as a function of H in two different orientations: $\theta_H = 0°$ (thick lines) and $\theta_H = 90°$ (thin lines) at fixed Ts (a) $T \leq 50$ K and (b) $T \geq 75$ K. At each T, H_p^c is clearly visible in both panels but in (b) H_p^{ab} is hard to identity because of the large y-axis scale. (c) The normalized in-plane MR, $\Delta\rho/\rho_0 = [\rho(H) - \rho_0]/\rho_0$ with $\rho_0 = \rho(H = 0)$ as a function of T measured at $\mu_0 H = 7$ T. $T_C = 133$ K is marked with an arrow. Blurred blue line is centered at $T_A = 52$ K, which is determined from the temperature at which $\rho(\theta_H = 0, H_p^c)$ is no longer smaller that $\rho(\theta_H = 90°)$. However, since we intend T_A to indicate approximate T scale above which the difference between the two MRs diminishes, we refer to $T_A \approx 50$ K in the main text.

$[\rho(H, \theta_H) - \rho_0]/\rho_0$ with $\rho_0 = \rho(H = 0)$, at $\mu_0 H = 7$ T, where all of the spins are polarized along either orientation of H. The discrepancy of the in-plane MR between the two orientations is most striking at 2 K, where the reduction of MR with out-of-plane magnetization is three times larger than with in-plane magnetization. We will come back to this below. Also the H-independent resistivity values in $H > H_p^c$ and $H > H_p^{ab}$ for both H directions imply that all spins are polarized and the contribution of spin-disorder induced scattering is very little.

As T increases, this trend reverses around $T_A \approx 50$ K, and $\rho(H, \theta_H = 0°)$ becomes higher in the entire H range. T_A is empirically determined from the temperature at which $\rho(\theta_H = 0, H_p^c)$ is no longer smaller than $\rho(\theta_H = 90°)$, as shown in Fig. 1(c). In $T > T_A$, the resistivity discrepancy between two spin polarization is overwhelmed by spin-disorder scattering induced resistance. This is also clear from the H dependence of two resistivities are parallel to each other in $T > T_A$ in Fig. 1(b).

The out-of-plane polarization field H_p^c is clearly identified up to T_C, as is H_p^{ab}, although the large x-axis scale makes it hard to identify in Fig. 1(b). At any given T, the lower polarization field for $\theta_H = 90°$ indicates a more effective suppression of spin-disorder for the same strength of H. This also gives rise to a lower ρ value in entire H range for high Ts. The similar rate of reduction of ρ at higher T, which makes the two curves at each temperature almost parallel, implies that their H dependence is attributed to the suppression of spin disorder.
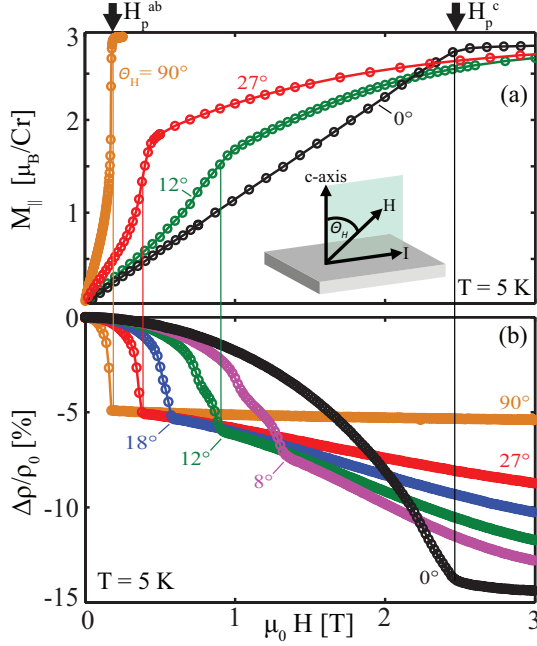

FIG. 2: (a) The magnetization component parallel to the applied magnetic field ($M_\parallel$) as a function of H at different angle θ_Hs at $T = 5$ K. The measurement configuration is shown in the inset. (b) In-plane MR as a function of H oriented at angle θ_H and $T = 5$ K. Vertical lines mark the polarization field ($H_p^{\theta_H}$) at a given θ_H. At intermediate angles, all spin are polarized at $H_p^{\theta_H}$ but are not yet aligned along H direction [26].

In Fig.2 (a) we plot the magnetization along the H direction ($M_\parallel$) as a function of H for different θ_Hs, at $T = 5$ K $\ll T_C$. The polarization fields ($H_p^{\theta_H}$) are clearly visible, indicated with vertical lines and with arrows for both end angles of $\theta_H = 0$ and $90°$. It occurs at fields well approximated by $H_p^{\theta_H} \simeq \frac{H_p^{ab}}{\sin \theta_H}$ [26]. The rapid rise in magnetization observed at large angles e.g. $\theta_H = 90°$ or $27°$ indicates a phase transition from the chiral soliton lattice to the ferromagnetic ordering. At intermediate angles, the rise at $H_p^{\theta_H}$ is not as rapid as at $\theta_H = 90°$. While all spins are polarized when $H = H_p^{\theta_H}$ at these angles, they are not yet aligned to the direction of H, but remain closer to the ab-plane. Upon increasing H more, the polarized spins collectively rotate until they

eventually align to H. This results in the gradual rise of $M_\parallel$ in $H > H_p^{\theta_H}$ toward the saturated value, which is ascribed to the competition between Zeeman and the magnetic anisotropy energy [26].

In Fig. 2 (b), we compare this with the in-plane MR. At $\theta_H = 90°$, the reduction in MR by 5.6% indicates a decrease in spin scattering as the helical ordering becomes polarized along H. A clear kink denotes the spin-polarization field H_p^{ab}. This dome-like shape is commonly observed in other helimagnets for the same reason [27, 28]. Once the spins completely polarize within the plane ($H > H_p^{ab}$), there is little variation in MR with H, which ensures that the contribution of the spin-disorder induced MR is negligible. It is worth pointing out that $\Delta\rho/\rho_0$ at $\theta_H = 90°$ bears great similarity, in both H dependence and magnitude, to that of the interlayer MR, i.e. the MR when I is applied along the c axis and H is in the ab plane, reported in [15].

When θ_H approaches 0, upon increasing H, the MR decreases much slower initially but eventually surpasses the in-plane value, reaching down to 14.1%, almost 3 times more reduction than $\theta_H = 90°$. This reduction is remarkable compared to the variation found in a typical traditional AMR phenomena, which are only a few tenths to a couple of percent at most [25]. Although slightly larger than a couple of percent out-of-plane AMR values have been reported in magnetic thin films systems [23], it is attributed to the reduction of spin scattering due to the geometrical size and texture of films. It is only very recent that the interface effect between adjacent magnetic and non-magnetic film was identified for a possible source of the out-of-plane AMR effect, yet the reported size is less than 1% [24].

For $\theta_H = 8°$ and $12°$ there is another kink in the MR, appearing in the range of H where the phase transition from chiral soliton lattice to ferromagnetic ordering occurs [15]. This finite width of the transition, only occurring for angles close to the c-axis, is believed to be caused by the formation of multiple domains undergoing the transition at slightly different fields, as also seen in $M_\parallel(H)$ of Fig.2 (a). While these kinks indicate a great sensitivity of the electrical transport to changes in the spin structure, it does not account for the continued decrease in MR in $H > H_p^{\theta_H}$.

To have a better understanding of this spin-orientation dependent in-plane MR, we examine the AMR effect in both in-plane and out-of-plane rotation of applied field. Schematics of the measurement are shown in insets of Fig.3. In the main panel, both in-plane and out-of-plane angular dependence of the in-plane resistivity normalized with $\rho_\parallel = \rho(\varphi_M = 0, \mu_0 H = 7\ T)$ are plotted, where φ_M denotes the angle between M and I (see Supplementary Materials [29]). In both cases, rotation of the magnetization give rise to a $\cos^2 \varphi_M$ angular dependences indicated with solid lines. However, the normalized AMR oscillation amplitude for the out-of-plane MR is larger by 23
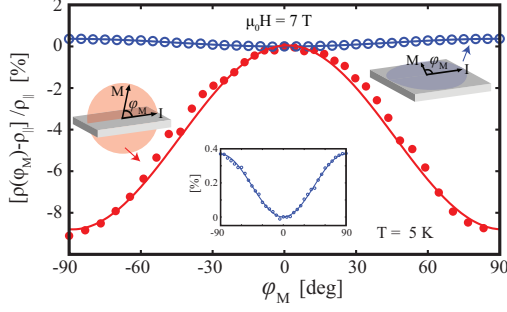
FIG. 3: In-plane MR at $\mu_0 H = 7$ T, normalized with $\rho_\parallel(\varphi_M = 0, \mu_0 H = 7\,T)$, where φ_M denotes the angle between the current and M both in-plane (open) and out-of-plane (closed circle), as shown in the sketches. Note the amplitude of out-of-plane AMR is 23 times larger than in-plane AMR. The angular dependences for both cases are found $\propto \cos^2 \varphi_M$, of which is displayed in the solid lines. Inset is plotted in-plane AMR with magnified y-axis.

FIG. 4: (a) H dependence of ρ_{yx} at various Ts below (solid lines) and above (broken lines) T_C. Peculiar concave H-dependence occurs only in $T < T_A \approx 50$ K. Since $H \parallel c$, all spins get *smoothly* polarized along c-axis via helical and conical state as H increases. (b) The ordinary (R_H) and anomalous (S_H) Hall coefficients, determined from fits of ρ_{yx}. Above T_A, both R_H and S_H are independent of T. Below T_A, the fit no longer works and S_H cannot be obtained in a reliable way. R_H is extracted from $\mu_0 H > 3$ T where ρ_{yx} is linear to H. (c) H dependence of ρ_{yx} less the OHE. AHE contribution decreases as T is lowered and is replaced with the hump-like feature in $T < T_A$, which has very little resemblance with $M(H)$. The curve for 50 K displays a little dip before becoming flat, displaying the crossover between the hump-like shape and AHE component.

times than the in-plane one; $+0.4\%$ and -9.1% change relative to $\rho_\parallel$ for in-plane and out-of-plane respectively. Note the different sign indicates the most reduced resistivity occurs when $M \parallel I$ for in-plane and $M \perp I$ for out-of-plane. This out-of-plane AMR effect should also be distinguished from giant magnetoresistance of magnetic multilayers, in which the saturated MR remain the same for both orientations [30].

Finally, we examine the Hall effect which is measured with H applied along c-axis ($\theta_H = 0$). This configuration matches those in which a topological Hall effect (THE) was observed in other helimagnets, e.g. with H along the helical axis [28]. Fig. 4 (a) shows field sweeps of the Hall resistivity (ρ_{yx}) at various fixed Ts. At low temperatures, an unexpected H dependence of ρ_{yx} emerges, characterized by the pronounced concave curvature for $0 < H < H_p^c$. As shown in Fig.4(c), this peculiar dependence is more obvious after subtracting the ordinary Hall contribution, as described in the forthcoming analysis. Note that this behavior emerges below $T_A \approx 50$ K, coinciding with the emergence of the MR discrepancy described above.

For $T > T_A$, the Hall signal exhibits archetypical anomalous Hall behavior, empirically expressed as $\rho_{yx}(H) = \mu_0 R_H H + \mu_0 R_s M$, where μ_0 is the vacuum permeability, R_H normal Hall coefficient, and R_s the anomalous Hall coefficient. The first and second terms correspond to the ordinary Hall effect (OHE) and the anomalous Hall effect (AHE), respectively. As T decreases, the AHE signal becomes visible at $T = 150$ K, and grows more prominent through T_C, where it is marked by a sharp kink at $H = H_p^c$. From the shape of the curves R_S has the opposite sign as R_H. In the limit of the intrinsic AHE, we can rewrite the anomalous Hall coefficient as $R_S = S_H \rho^2(T, H)$, with S_H an H in-
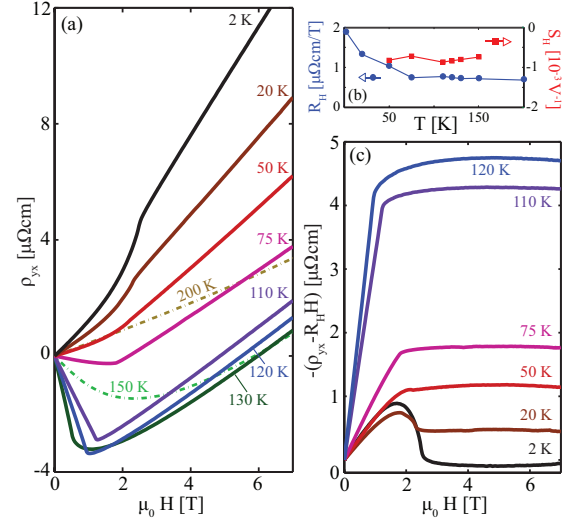
dependent constant [27], and fit our $\rho_{yx}(H)$ traces well in $T_A < T \leq T_C$. The fitting parameters R_H and S_H are plotted in Fig.4 (b). The effective carrier density derived from R_H in $T > T_A$ is found 9×10^{20} holes/cm^3. It is consistent with the value found above T_C at 200 K, where the Hall signal recovers almost a linear H dependence.

In $T < T_A$ however, this analysis is no longer valid and cannot capture the concave H dependence, even when an additional extrinsic contribution term is included. As seen in Fig.4 (c), the emergence of a novel H dependence below H_p^c replaces the gradual reduction of the AHE contribution. It is hard to connect it with the AHE picture, as it bears no resemblance to $M(H)$. We rule out the possibility that this behavior is caused by the topological Hall effect (THE) [2, 3] for the following reasons: first our spin structure model found the skyrmion density is zero in this material for any temperature and the formation of skyrmions is unlikely due to the large magnetic anisotopy [26]. Second, the T dependence – occurring at low Ts and vanishing as T increases – is the opposite to what was observed in the THE in other magnetic systems [28]. Lastly, a recent neutron scattering study

could not identify the existence of a complex periodic spin structure of skyrmions [22].

It is interesting to compare the Hall effect of $Cr_{1/3}NbS_2$ to that of $Fe_{1/4}TaS_2$, an anisotropic magnetic dichalcogenide with a similar crystalline structure. Both have the same resistivity at 5 K, but $Cr_{1/3}NbS_2$ has one-tenth the carrier density of $Fe_{1/4}TaS_2$. This means the $Cr_{1/3}NbS_2$ has a ten-fold larger mean free path (l). The intrinsic AHE signal scales with $1/l^2$ and diminishes rapidly as T is lowered and ρ decreases [27], resulting in the OHE dominating the Hall signal at low temperatures, i.e. a recovery of H linear dependence of ρ_{yx}. This is consistent with our observation that the extrinsic AHE is negligible over the entire temperature range in $Cr_{1/3}NbS_2$[31].

The fact that unusual H profile of ρ_{yx} and the larger amplitude of out-of-plane AMR occur in the same T range, $T < T_A \approx 50$ K, implies that the two phenomena share a similar origin. In this temperature regime R_H, which was estimated from the slope of ρ_{yx} when $H > 3$ T, increases rapidly. The crossover temperature T_A also appeared in other measurements: the T dependence of the thermopower [29] changes slowly just below T_C, and then after a broad shoulder around 50 K rapidly decreases. These unusual spin-orientation dependent transport features, unique to $Cr_{1/3}NbS_2$, emerge only below T_A. T_A is also consistent with a deviation from Bloch's $T^{3/2}$ law of $M(T)$[13]. These observations points to a spin-orbit coupling effect of order $k_B T_A$, with k_B the Boltzmann constant.
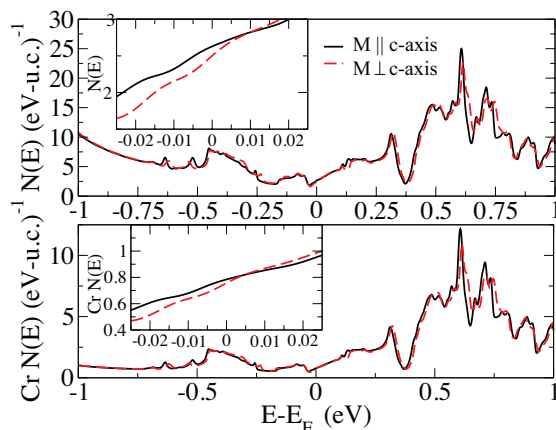

FIG. 5: The calculated magnetic density-of-states of $Cr_{1/3}NbS_2$ for the indicated magnetic moment orientations; (a) total DOS, (b) Cr DOS. The energy scale $\pm$ 25 meV centered at Fermi energy E_F is magnified in the insets. The DOS at E_F was found to be 3.2 % greater when the moments orient along the c-axis instead of perpendicular to it, while the in-plane plasma frequencies are essentially unaffected by magnetization orientation, which is consistent with enhanced conductivity within an order of unity.
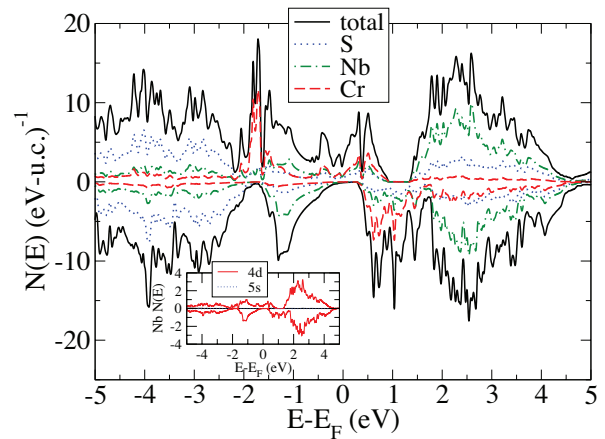

FIG. 6: The calculated magnetic density-of-states of $Cr_{1/3}NbS_2$ projected by spin and atomic character. Inset: the orbital-projected character of the Nb DOS.

In an attempt to understand these anisotropic magnetotransport properties, first principles calculations were pursued (procedural details in [29]). Results of these calculations, depicted in Fig. 5 show a significant dependence of the calculated magnetic density of states on moment orientation, both for the total DOS (top) and Cr DOS (bottom). As indicated in the inset to Fig. 5, for states very near the Fermi level (E_F) – less than 25 meV from E_F - the DOS can vary by as much as 15% depending on moment orientation. Moreover, the Fermi level density of state (DOS) was found to be 3.2 % greater when the moments orient along the c-axis instead of perpendicular to it, while the in-plane plasma frequencies are essentially unaffected by magnetization orientation. Thus, neglecting spin-orientation dependent scattering processes, the increase in DOS is largely responsible for the reduction of the in-plane resistivity when the magnetization lies parallel to the c-axis instead of the ab-plane. The resistivities for the two spin-polarization directions at 5 K differ by 11%, which is bigger than the DOS difference by a factor of the order of unity. Also, by examining the bands near E_F (within a 20 meV window) for both orientations, one finds the averaged offset in the energies to be approximately 1.7 meV $\simeq$ 20 K. This is a direct result of SOC and consistent with the temperature scale T_A found in the MR and Hall effect data. These changes in electronic structure and their subsequent modification of scattering processes are likely responsible for the spin orientation dependence in the transport.

We note also from Fig. 5 that the Cr-site DOS is of essentially the same shape as the total DOS, within an eV of E_F. In addition, the effects on the Cr DOS of the change in moment orientation from [001] ($\parallel c$) to [100] ($\parallel ab$) closely parallel the changes in the total DOS. This is due to the primary role of the Cr atoms in the magnetic behavior - only for atoms with a large local moment, such

as the Cr here, does one expect a moment-orientation dependent DOS. Note that in the calculation the induced Nb moment is only 0.05 μ_B and that on S essentially zero.

In Figure 6 we show the magnetic state DOS projected into spin-up and spin-down sub-bands, along with the Nb $4d$ and $5s$ orbital-projected DOS. A substantial exchange splitting is visible in the Cr DOS, as expected given its magnetic character, with some minor splitting also observed in the Nb and S. There is little, if any, spin-down character to the Cr DOS for nearly 2 eV below E_F. This is suggestive of the strength of the magnetism in this system, as indicated by the 3 μ_B/Cr total magnetic moment found both in the calculation and the experiment. There is substantial hybridization around E_F, indicative of covalent bonding, although the Cr states are generally confined to within 2 eV of E_F and the Nb and S predominate outside this range. In the inset of Figure 6 we plot the orbital-projected Nb DOS, which is dominated by $4d$ contributions, with the $5s$ contribution negligible.

Further detailed investigation on the electronic structure depending on the spin direction will shed light on understanding the difference of amplitudes of in-plane and out-of-plane AMR. This mechanism is suspected to be closely related to abnormal H dependence of the Hall effect observed for $T < T_A$.

The remarkable sensitivity of the magnetotransport behavior to polarized spin orientation in $Cr_{1/3}NbS_2$ is mostly driven by Cr^{3+} ions. Strong magnetization orientation dependence of the electronic structure of $3d$ metals leads to large effects on the magnetotransport properties in $Cr_{1/3}NbS_2$. The same strong dependence also underlies efforts to control magnetic anisotropy in multilayer systems made of $3d$ magnetic elements. Our results demonstrates a closely interwoven relation among the orientation of magnetization, the resultant electronic structure change and its influence on the electrical conduction, all of which are mediated by spin-orbit coupling. Furthermore, the non-collinear helical ground state enriches the role of spin-orbit coupling and the subsequent complexity of the electrical transport properties.

†Current Address: Los Alamos National Laboratory, Los Alamos, NM

* Electronic address: minhyea.lee@colorado.edu

[1] S. Muhlbauer, B. Binz, F. Jonietz, C. Pfleiderer, A. Rosch, A. Neubauer, R. Georgii, and P. Boni, Science **323**, 915 (2009).

[2] M. Lee, W. Kang, Y. Onose, Y. Tokura, and N. P. Ong, Phys. Rev. Lett. **102**, 186601 (2009).

[3] A. Neubauer, C. Pfleiderer, B. Binz, A. Rosch, R. Ritz, P. G. Niklowitz, and P. Böni, Phys. Rev. Lett. **102**, 186602 (2009), URL http://link.aps.org/doi/10.1103/PhysRevLett.102.186602.

[4] I. Dzyaloshinsky, Journal of Physics and Chemistry of Solids **4**, 241 (1958), ISSN 0022-3697, URL http://www.sciencedirect.com/science/article/pii/0022369758900763.

[5] T. Moriya, Phys. Rev. **120**, 91 (1960), URL http://link.aps.org/doi/10.1103/PhysRev.120.91.

[6] J. M. Hopkinson and H.-Y. Kee, Phys. Rev. B **79**, 014421 (2009), URL http://link.aps.org/doi/10.1103/PhysRevB.79.014421.

[7] A. Fert, V. Cros, and J. Sampaio, Nature nanotechnology **8**, 152 (2013).

[8] N. Romming, C. Hanneken, M. Menzel, J. E. Bickel, B. Wolter, K. von Bergmann, A. Kubetzka, and R. Wiesendanger, Science **341**, 636 (2013).

[9] B. C. Sales, R. Jin, and D. Mandrus, Phys. Rev. B **77**, 024409 (2008), URL http://link.aps.org/doi/10.1103/PhysRevB.77.024409.

[10] Y. Mokrousov, H. Zhang, F. Freimuth, B. Zimmermann, N. H. Long, I. Weischenberg, J.and Souza, P. Mavropoulos, and S. Blugel, J. Phys.: Cond. Matt. **25**, 163201 (2013).

[11] N. J. Ghimire, M. A. McGuire, D. S. Parker, B. Sipos, S. Tang, J.-Q. Yan, B. C. Sales, and D. Mandrus, Phys. Rev. B **87**, 104403 (2013), URL http://link.aps.org/doi/10.1103/PhysRevB.87.104403.

[12] T. Moriya and T. Miyadai, Solid State Comm. **42**, 209 (1982).

[13] T. Miyadai, K. Kikuchi, H. .Kondo, S. Sakka, M. Arai, and Y. Ishikawa, J. Phys. Soc. Jpn. **52**, 1394 (1983).

[14] Y. Togawa, T. Koyama, K. Takayanagi, S. Mori, Y. Kousaka, J. Akimitsu, S. Nishihara, K. Inoue, A. S. Ovchinnikov, and J. Kishine, Phys. Rev. Lett. **108**, 107202 (2012), URL http://link.aps.org/doi/10.1103/PhysRevLett.108.107202.

[15] Y. Togawa, Y. Kousaka, S. Nishihara, K. Inoue, J. Akimitsu, A. S. Ovchinnikov, and J. Kishine, Phys. Rev. Lett. **111**, 197204 (2013), URL http://link.aps.org/doi/10.1103/PhysRevLett.111.197204.

[16] H. Brooks, Phys. Rev. **58**, 909 (1940), URL http://link.aps.org/doi/10.1103/PhysRev.58.909.

[17] P. Bruno, Phys. Rev. B **39**, 865 (1989), URL http://link.aps.org/doi/10.1103/PhysRevB.39.865.

[18] D.-s. Wang, R. Wu, and A. J. Freeman, Phys. Rev. B **47**, 14932 (1993), URL http://link.aps.org/doi/10.1103/PhysRevB.47.14932.

[19] M. Bode, S. Heinze, A. Kubetzka, O. Pietzsch, X. Nie, G. Bihlmayer, S. Blügel, and R. Wiesendanger, Phys. Rev. Lett. **89**, 237205 (2002), URL http://link.aps.org/doi/10.1103/PhysRevLett.89.237205.

[20] F. Gimbert and L. Calmels, Phys. Rev. B **86**, 184407 (2012), URL http://link.aps.org/doi/10.

1103/PhysRevB.86.184407.

[21] K. Hotta, K. Nakamura, T. Akiyama, T. Ito, T. Oguchi, and A. J. Freeman, Phys. Rev. Lett. **110**, 267206 (2013), URL http://link.aps.org/doi/10.1103/PhysRevLett.110.267206.

[22] N. J. Ghimire, Ph.D. thesis, University of Tennessee (2013).

[23] T. G. S. M. Rijks, S. K. J. Lenczowski, R. Coehoorn, and W. J. M. de Jonge, Phys. Rev. B **56**, 362 (1997), URL http://link.aps.org/doi/10.1103/PhysRevB.56.362.

[24] A. Kobs, S. Heße, W. Kreuzpaintner, G. Winkler, D. Lott, P. Weinberger, A. Schreyer, and H. P. Oepen, Phys. Rev. Lett. **106**, 217207 (2011), URL http://link.aps.org/doi/10.1103/PhysRevLett.106.217207.

[25] T. McGuire and R. Potter, IEEE Trans. Magn. **11**, 101838 (1975).

[26] B. J. Chapman, A. Bornstein, N. J. Ghimire, D. Mandrus, and M. Lee, Applied Physics Letters **105**, 072405 (2014).

[27] M. Lee, Y. Onose, Y. Tokura, and N. P. Ong, Phys. Rev. B **75**, 172403 (2007), URL http://link.aps.org/doi/10.1103/PhysRevB.75.172403.

[28] B. J. Chapman, M. G. Grossnickle, T. Wolf, and M. Lee, Physical Review B **88**, 214406 (2013).

[29] See Supplemental Material at [URL will be inserted by publisher] for thermopower measurement, Out of plane AMR and details of first principle calculations.

[30] M. N. Baibich, J. M. Broto, A. Fert, F. N. Van Dau, F. Petroff, P. Etienne, G. Creuzet, A. Friederich, and J. Chazelas, Phys. Rev. Lett. **61**, 2472 (1988), URL http://link.aps.org/doi/10.1103/PhysRevLett.61.2472.

[31] The second term $\rho_{yx} = \mu_0 R_H H + \mu_0 R_s M$ was modified to $\mu_0 S_H \rho^2 M \left(1 + \frac{\rho_I}{\rho}\right)$, with ρ_I an additional fitting parameter, but fits revealed $\frac{\rho_I}{\rho} \ll 1$ over most of the T range investigated. Meanwhile, in $Fe_{1/4}TaS_2$, ρ_{xy} is dictated by the intrinsic AHE at low T and then the extrinsic AHE as T approaches T_C.

[32] P. Blaha et al., *WIEN2k, An Augmented Plane Wave + Local Orbitals Program for Calculating Crystal Properties* (North-Holland Pub. Co., 2001).

[33] J. P. Perdew, K. Burke, and M. Ernzerhof, Physical Review Letters **78**, 1396 (1997).